Acta Crystallographica Section D
Biological Crystallography
ISSN 0907-4449

Structures of the Dsk2 UBL and UBA domains and their complex

Edward D. Lowe, Na'il Hasan,‡ Jean-Francois Trempe, Laura Fonso, Martin E. M. Noble, Jane A. Endicott, Louise N. Johnson and Nick R. Brown*

Laboratory of Molecular Biophysics, Department of Biochemistry, University of Oxford, Oxford OX1 3QU, England

‡ Present addess: Department of Biology and Biochemistry, Birzeit University, West Bank, Palestine.

Correspondence e-mail: nick@biop.ox.ac.uk

Received 7 September 2005
Accepted 16 November 2005

PDB References: Dsk2 UBL, 2bwf, r2bwfsf; Dsk2 UBA, 2bwb, r2bwbsf; Dsk2 UBA–UBL complex, 2bwe, r2bwesf.

The yeast proteins Dsk2 and Rad23 belong to a family of proteins that contain an N-terminal ubiquitin-like domain (UBL) and a C-terminal ubiquitin-associated domain (UBA). Both Dsk2 and Rad23 function as adaptors to target ubiquitin-labelled proteins to the proteasome through recognition of polyubiquitin (four or more K48-linked ubiquitins) by their UBA domains and to the yeast proteasomal subunit Rpn1 by their UBL domains. The crystal structures of the Dsk2 UBL domain, the Dsk2 UBA domain and the Dsk2 UBA–UBL complex are reported. In the crystal, the Dsk2 UBA domains associate through electrostatic interactions to form ninefold helical ribbons that leave the ubiquitin-binding surface exposed. The UBA–UBL complex explains the reduced affinity of the UBA domain for UBL compared with ubiquitin and has implications for the regulation of Dsk2 adaptor function during ubiquitin-mediated proteasomal targeting. A model is discussed in which two or more Dsk2 UBA molecules may selectively bind to K48-linked polyubiquitin.

1. Introduction

Ubiquitin-mediated protein degradation provides a major mechanism for controlled proteolysis of targeted proteins. Ubiquitin (Ub), consisting of 76 amino-acid residues, is conserved in all eukaryotes and is implicated in a wide range of cellular regulatory functions including protein degradation, transcriptional control and DNA repair (Hershko & Ciechanover, 1998). In these processes, ubiquitin is attached to a target protein by an isopeptide linkage between its C-terminal carboxyl group and a lysine ε-amino group of the target protein or another Ub molecule. The attachment is catalysed by a cascade of enzymes (Pickart, 2001). The consequences of Ub attachment depend upon how many Ub moieties are attached and the cross-links involved. Recognition for degradation by the proteasome involves polyubiquitin chains of at least four molecules in length (Thrower *et al.*, 2000) in which each ubiquitin is linked *via* an isopeptide bond from the carboxy-terminus of one ubiquitin to K48 on the adjacent ubiquitin (Chau *et al.*, 1989). (The single-letter amino-acid code is used throughout this paper.) Other cross-links through K63 and K29 are also found that may be important for other processes. A proteomics screen of ubiquitin conjugates in *Saccharomyces cerevisiae* found ubiquitin modified at all seven lysine residues (Peng *et al.*, 2003).

The 26S proteasome consists of the 20S core complex, composed of four stacked rings of seven subunits that contain the proteolytic sites in the central cavity (Groll *et al.*, 1997), and a multisubunit 19S regulatory particle that caps both ends

of the 20S particle. The 19S particle, comprising a lid, a linker and a base, mediates the recognition of polyubiquitinated targeted proteins and promotes their unfolding in an ATP-dependent reaction. The base contains eight subunits (six ATPases of the AAA family and two large subunits, S2/Rpn1 and S1/Rpn2) and is connected to the lid by the S5a/Rpn10 protein (Ferrell *et al.*, 2000) (using the human/*S. cerevisiae* nomenclatures, respectively).

S. cerevisiae Dsk2 and its human orthologues PLIC-1 and PLIC-2 are members of a family of proteins that contain both an N-terminal Ub-like (UBL) domain and a C-terminal Ub-associated (UBA) domain (Fig. 1). The family includes Rad23 and its human orthologues hHR23A and hHR23B, which are involved in nucleotide-excision repair of damaged DNA and ubiquitin-mediated proteolysis. *DSK2* was originally isolated as a suppressor of *kar1*, which is defective in spindle-pole duplication (Biggins *et al.*, 1996). Dsk2 and Rad23 have 17% identity in sequence overall (23% for their UBL domains; 29 and 19% for the UBA domains 1 and 2 of Rad23, respectively) and differ markedly in the region that separates their UBL and UBA domains. This intervening sequence in yeast Dsk2, which is also shared by its human and *Xenopus* orthologues, has a weakly repetitive character showing distant similarity to Sti1, an Hsp70-binding protein (Funakoshi *et al.*, 1999; Kaye *et al.*, 2000). In contrast, the Rad23 intervening sequence bears a xeroderma pigmentosum C (XPC) binding domain essential for its excision-repair function (Masutani *et al.*, 1997). Deletion of *DSK2* is not lethal, but yeast strains in which both *DSK2* and *RAD23* are deleted are temperature-sensitive for growth because of a block on spindle-pole body duplication (Biggins *et al.*, 1996). Further synthetic phenotypic defects among mutants of Dsk2 and Rad23 suggest that these proteins perform overlapping functions (Elsasser *et al.*, 2004).

The UBL domains mediate the interactions of Dsk2, Rad23 and their orthologues with the proteasome (Elsasser *et al.*, 2004; Funakoshi *et al.*, 2002; Kleijnen *et al.*, 2003; Schauber *et al.*, 1998). In higher eukaryotes, the S5a subunit binds the UBL domain *via* its UIM motifs (Hiyama *et al.*, 1999). In *S. cerevisiae*, the corresponding subunit, Rpn10, lacks the second UIM and *rpn10* deletion mutants are viable (van Nocker *et al.*, 1996). Like Rad23, the Dsk2 UBL domain has been found to interact with Rpn1 (Elsasser *et al.*, 2002; Saeki *et al.*, 2002; Seeger *et al.*, 2003), a subunit (corresponding to S2 in higher eukaryotes) of the base subcomplex of the 19S regulatory component of the proteasome. The UBL domain (reviewed in Walters *et al.*, 2004) shares the ubiquitin fold (Vijay-Kumar *et al.*, 1987) comprised of a five-stranded antiparallel β-sheet and one α-helix. The β-sheet constitutes one face of the protein and bears a hydrophobic patch that has been implicated in interactions with the proteasome (Walters *et al.*, 2002).

The UBA domain, first identified from a bioinformatics analysis (Hofmann & Bucher, 1996), consists of approximately 45 residues and is found in many proteins of the ubiquitin/proteasome pathway. Most UBA domains bind to Ub and to polyubiquitin chains (Bertolaet *et al.*, 2001; Funakoshi *et al.*, 2002; Rao & Sastry, 2002; Wilkinson *et al.*, 2001), but not all (Davies *et al.*, 2004). *In vivo*, Dsk2 UBA domain binds K48-linked poly-Ub chains, the predominant form of poly-Ub in cells (Funakoshi *et al.*, 2002). A recent survey of UBA-domain selectivity, using a GST UBA-domain pull-down assay, indicated that isolated Dsk2 UBA domains are relatively non-selective for K48- or K63-linked tetraubiquitin (Raasi *et al.*, 2005).

UBA domains are one of a number of Ub-binding families, which include the Ub-interacting motif (UIM) and the coupling of Ub conjugation to ER degradation (CUE) domains. Structures have been determined for all three types of module (Ciani *et al.*, 2003; Kang *et al.*, 2003; Mueller & Feigon, 2002; Prag *et al.*, 2003; Withers-Ward *et al.*, 2000; Ohno *et al.*, 2005; Trempe *et al.*, 2005). The first UBA structure [of the hHR23A UBA(2) domain] showed a three-helix bundle with a hydrophobic patch that is now known to mediate protein–protein interactions (Dieckmann *et al.*, 1998). Chemical shift perturbation experiments have allowed binding interfaces to be inferred for the UBA domains from hHRA23A and B (Mueller *et al.*, 2004; Ryu *et al.*, 2003; Wang *et al.*, 2003). This information has been confirmed and extended by the complex structures of Cue2–Ub (Kang *et al.*, 2003), Vps9–Ub (Prag *et al.*, 2003) and Dsk2 UBA–Ub (Ohno *et al.*, 2005). More recently, NMR data has led to proposed structures for human HR23A (Varadan *et al.*, 2005) and *Schizosaccharomyces pombe* Mud1 (Trempe *et al.*, 2005) UBA domains in association with K48-linked Ub_2 in which the closed conformation of K48 Ub_2 forms a sandwich-like structure with the UBA.

An adaptor model for Dsk2 and Rad23 (and their orthologues) has been proposed in which these proteins deliver polyubiquitinated substrates to the proteasome through binding of the UBA domain to poly-Ub and interaction of the UBL domain with subunit(s) of the 19S proteasomal base (Hartmann-Petersen *et al.*, 2003; Madura, 2004). UBA domains also bind to UBL domains, albeit less strongly than Ub, and chemical shift perturbation experiments suggest the interface to be similar to that for Ub itself (Ryu *et al.*, 2003). The intramolecular interaction between UBA/UBL domains may play a role in regulation of binding activity (Walters *et al.*, 2003).

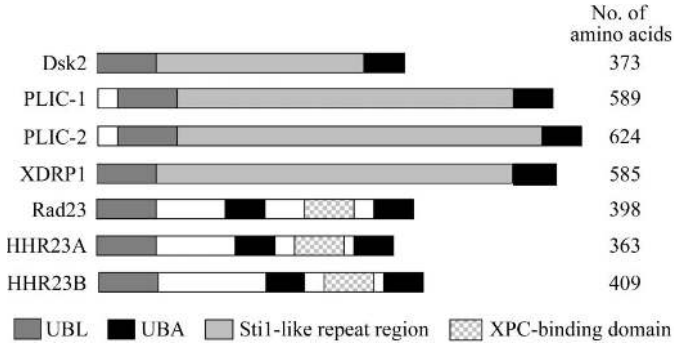

Figure 1
Schematic representation of the domain structure for *S. cerevisiae* Dsk2, the human orthologues PLIC-1 and PLIC-2, the *Xenopus* orthologue XRDP1 and the DNA damage-response proteins *S. cerevisiae* Rad23 and the human orthologues hHR23A and hHR23B.

Table 1
Summary of data-processing and refinement statistics for Dsk2 UBL domain, Dsk2 UBA domain and the Dsk2 UBA–UBL complex.

Values in parentheses are for the highest resolution shell. NA, not applicable.

		UBA domain			
	UBL domain	Peak (0.97904 Å)	High-energy remote (0.90736 Å)	Native	UBA–UBL complex
Data collection					
Synchrotron source	ESRF ID14-EH1	ESRF BM16	ESRF BM16	ESRF ID14-EH1	ESRF ID14-EH2
Space group	$P2_12_12_1$	$C2$	$C2$	$C2$	$P2$
Unit-cell parameters					
a (Å)	49.415	119.181	119.181	116.303	76.232
b (Å)	49.587	44.366	44.366	44.038	90.647
c (Å)	58.771	111.937	111.937	111.501	140.84
β (°)		114.953	114.953	114.884	106.22
Resolution (Å)	37.8–1.15 (1.21–1.15)	41.0–3.2 (3.37–3.2)	41.0–3.2 (3.37–3.2)	29.4–2.3 (2.42–2.3)	59.2–3.10 (3.27–3.10)
No. of reflections	217953	58255	58860	83285	111432
No. of unique reflections	48617	9023	8997	23110	33693
Mean $I/\sigma(I)$	14.7 (2.5)	14.9 (4.0)	14.7 (3.2)	16.8 (3.9)	11.5 (3.5)
Completeness (%)	93.8 (81.2)	99.9 (100.0)	99.7 (98.8)	99.8 (100.0)	99.1 (99.6)
Anomalous completeness (%)	NA	99.4 (99.6)	99.1 (96.3)	NA	NA
Multiplicity	4.5 (2.5)	6.5 (6.4)	6.5 (5.7)	3.6 (3.6)	3.3 (3.3)
Anomalous multiplicity	NA	3.4 (3.3)	3.4 (3.0)	NA	NA
R_{sym}	0.077 (0.289)	0.114 (0.339)	0.117 (0.391)	0.056 (0.277)	0.10 (0.496)
Wilson B factor (Å^2)	9.6	75.7	76.1	54.1	79.3
Phasing					
Phasing power (dispersive/anomalous)	NA	NA/1.832	2.068/0.857	NA	NA
R_{cullis} (dispersive/anomalous)	NA	NA/0.655	0.493/0.879	NA	NA
FOM_{final}	NA	0.661		NA	NA
Refinement					
Protein atoms	1211			3164	8310
Waters	159			175	101
R_{conv}	0.182			0.243	0.240
R_{free}	0.193			0.307	0.266
Mean B factor (Å^2)	15.5			72.4	71.4
R.m.s.d. bond lengths (Å)	0.009			0.011	0.015
R.m.s.d. bond angles (°)	1.37			1.15	1.58
Ramachandran plot					
Most favoured region (%)	94.2			95.8	90.7
Additionally allowed (%)	5.8			4.2	9.1
Generously allowed (%)	0			0	0.2
Disallowed (%)	0			0	0

In this paper, we present the X-ray structures of isolated Dsk2 UBL and UBA domains at 1.15 and 2.3 Å resolution, respectively, and the crystal structure of the Dsk2 UBA–UBL complex at 3.1 Å resolution. We demonstrate a tenfold reduction in affinity of the UBA domain for UBL compared with Ub. The complex structure provides a molecular explanation for this reduced affinity and we discuss the implications for the regulation of Dsk2 adaptor function during Ub-mediated proteasomal targeting. Finally, we consider a model in which Dsk2 may selectively bind to a K48-linked poly-Ub chain with enhanced affinity.

2. Materials and methods

2.1. Expression and purification

Expression plasmids (pGEX-KG) encoding *S. cerevisiae* Dsk2 UBL domain (residues 1–77) and UBA domain (residues 328–373) were a gift from H. Kobayashi (Kyushu University, Japan). Protein expression in B834(DE3) pLysS cells was induced with 0.1 m*M* IPTG and allowed to proceed for 4 h at 310 K. GST-fusion proteins were purified from clarified lysates by glutathione Sepharose chromatography and cleaved with thrombin [1:10 000(*w*:*w*), 18 h at 293 K]. Digests were further purified by Superdex 75 chromatography. Bovine ubiquitin was purchased from Sigma.

Purified UBL and UBA domains were analysed with a Micromass BioQ II-ZS electrospray mass spectrometer (VG Biotech, UK) by R. Aplin (Oxford Centre for Molecular Sciences). For UBL, the observed molecular weight of 9745.58 ± 0.03 Da was consistent with the UBL domain residues 1–77 with an N-terminal extension of GSPGISGGGGGILD from the vector (calculated weight of 9743.98 Da). The UBA domain molecular weight was 6319.0 Da (predicted 6318.90 Da). The N-terminal sequences were confirmed by amino-acid sequencing (A. Willis, Department of Biochemistry, Oxford University).

2.2. Surface plasmon resonance experiments

The GST-UBA fusion was captured on a CM5 chip using immobilized anti-GST monoclonal antibody. Sensograms were recorded with a BIAcore 2000 instrument. The analyte (Ub or UBL) was passed over the chip with increasing concentrations

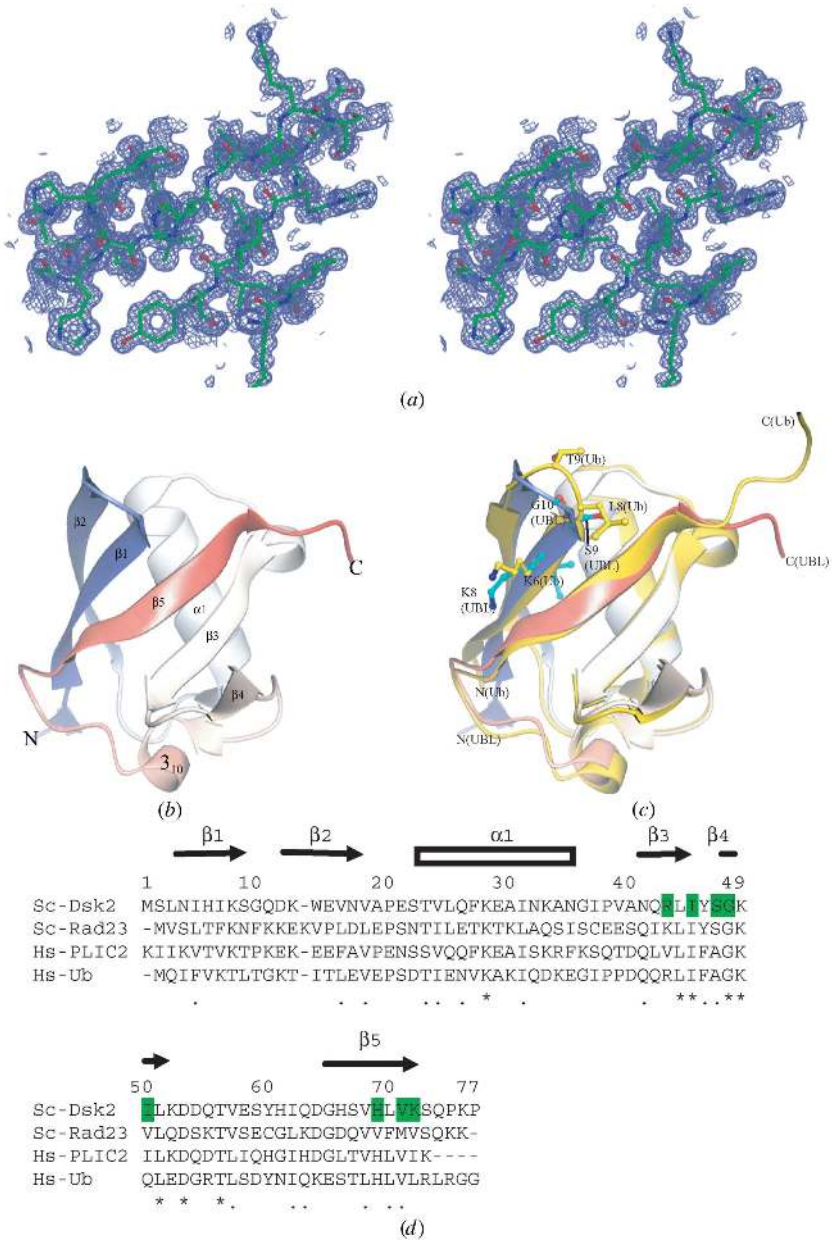

Figure 2
The structure of the Dsk2 UBL domain. (*a*) Stereo diagram of part of the 1.15 Å resolution σ_A-weighted $2F_o - F_c$ electron-density map contoured at 0.48 e Å^{-3}. Parts of β-strands $\beta1$, $\beta5$, $\beta3$ and $\beta4$ are shown. This figure and others were produced with *AESOP* (Martin Noble, unpublished program). (*b*) Schematic diagram of the Dsk2 UBL domain coloured blue to red from the the N-terminus to the C-terminus. Secondary-structural elements are labelled. $\beta1$, L3–S9; $\beta2$, D12–V18; $\alpha1$, T23–G36; $\beta3$, N41–Y46; $\beta4$, K49–L51; 3_{10}, E58–H61; $\beta5$, Q65–S73. (*c*) Comparison of the structure of Dsk2 UBL (coloured blue to red) with Ub (yellow). The major differences are in the loop between $\beta1$ and $\beta2$ (where the side chains of UBL residues 8–10 and Ub residues 6–9 are shown) and the C-terminal region. (*d*) The aligned sequences of UBL domains from *S. cerevisiae* Dsk2, *S. cerevisiae* Rad23, human PLIC2 and human ubiquitin. The secondary-structural elements for Dsk2 UBL are shown as rectangles for α-helices and arrows for β-strands. The symbols * and . below the sequences indicate identical and similar residues, respectively. Residues that contact the UBA domain in the UBA–UBL complex are highlighted in green.

(see supplementary material[1]). Measurements were made in triplicate for Ub and in duplicate for UBL. Control sensorgrams using captured GST were subtracted to produce the corrected sensorgrams. Data were analysed using the *BIAevaluation* software. K_d values were calculated from plots of the plateau response as a function of analyte concentration.

2.3. Crystallization and data collection

Proteins were prepared in HBS (10 m*M* HEPES pH 7.5, 150 m*M* NaCl, 3 m*M* EDTA, 0.01% monothioglycerol, 0.01% azide) and concentrated to 5–12 mg ml^{-1}.

UBL crystals were grown at 293 K with precipitant 1.3–1.6 *M* trisodium citrate pH 7.0 (pH adjusted with acetic acid). Crystals were cryoprotected using a 50:50 mixture of 8 *M* formate and 1 *M* sodium bromide. Data were collected to 1.15 Å resolution at ESRF ID14-1 and were processed with *MOSFLM* (Leslie, 1999) and *CCP*4 programs (Collaborative Computational Project, Number 4, 1994) (Table 1).

Native and SeMet UBA crystals were grown with precipitant 6–12% methoxy PEG 2K buffered with 0.1 *M* sodium acetate pH 5.3–5.7. Crystals were briefly cryoprotected with mother liquor supplemented with 30% ethylene glycol. Data to 2.3 Å were recorded for native UBA crystals at ESRF ID14-1 and data to 3.3 Å were recorded for SeMet UBA crystals at ESRF BM16 and processed as above (Table 1).

UBA–UBL complex crystals were grown from an equimolar mixture of UBA and UBL equilibrated against 10–15% methoxy PEG 5K buffered with 0.1 *M* MES pH 6.5 at 277 K. Crystals were cryoprotected with mother liquor containing 25% glycerol. Data to 3.1 Å were collected at ESRF ID14-2 and processed as above (Table 1).

2.4. Dsk2 UBL domain structure determination

The structure was solved by molecular replacement with *AMoRe* (Navaza, 1994) using the 1.7 Å structure (PDB code 1bt0) of the UBL domain from *Arabidopsis thaliana* Rub1 (Rao-Naik *et al.*, 1998; 34% sequence identity) as a search model. The structure (two molecules *A* and *B* per asymmetric unit) was improved by rounds of restrained refinement with *REFMAC* (Murshudov *et al.*, 1997) and identification of missing residues with *ACORN* (Foadi *et al.*, 2000). After inclusion of water molecules and six formate ions, the refined structure gave final R and R_{free} values of 0.194 and 0.201, respectively. Inclusion of H atoms at predicted

[1] Supplementary material has been deposited in the IUCr electronic archive (Reference: BE5044). Details for accessing these data are given at the back of the journal.

positions and anisotropic B factors led to a refined model with R and R_{free} values of 0.182 and 0.193, respectively (Table 1). The glutamine side chain of residue 11 in the A subunit was not visible in the electron-density map and the residue was built as alanine. The cores of the two Dsk2 UBL molecules in the asymmetric unit (molecules A and B) are nearly identical (the r.m.s.d. in C^{α} coordinates for residues 3–71 is 0.28 Å).

2.5. Dsk2 UBA structure determination

SeMet Dsk2 UBA data were collected at peak and high-energy remote wavelengths. Eight selenium sites were found using *SHELXD* (Schneidner & Sheldrick, 2002) and refined using *SHARP* (de La Fortelle & Bricogne, 1997). Density modification was carried out using *RESOLVE* (Terwilliger, 2000) and an initial model was built using *O* (Jones *et al.*, 1991). The model was refined (eight UBA molecules) against the higher resolution native data (2.3 Å resolution) and iterative rebuilding and refinement were carried out using *O* and *REFMAC*5 (Murshudov *et al.*, 1997). Tight NCS restraints were applied throughout refinement. A ninth molecule (molecule I) was built which was slightly different to the other eight molecules with changes induced from its proximity to the crystallographic twofold that results in residues 342–345, the region containing Met342, being disordered. The nine UBA molecules in the asymmetric unit are arranged in chains. Molecule A from one $ABCDI$ chain docks with a symmetry-related H' molecule from the $EFGH$ chain and molecule I from the $ABCDI$ chain docks to molecule E'' from the symmetry-related $EFGH$ chain to generate a chain $E'F'G'H'ABCDIE''F''G''H''$ *etc*. that extends throughout the crystal.

2.6. Dsk2 UBA/UBL structure determination

The Dsk2 UBA–UBL structure was solved by molecular replacement. A tetramer consisting of molecules A, B, C and D of the UBA structure was used as a search model and three copies of this tetramer were placed using *MOLREP* (Vagin & Teplyakov, 1997). Inspection of initial difference maps following rigid-body refinement showed the presence of two UBL molecules (chains S and T in the final refined structure). Further UBA molecules were located from difference density during subsequent rounds of refinement. In the final refined structure 18 UBA molecules are present, arranged in continuous helical chains. A third UBL molecule was found in difference density once all 18 UBA molecules were in place. This molecule (chain U in the final refined structure) is less well ordered than the other two UBL molecules. The structure was built and refined using cycles of *REFMAC*5 and *O*. Tight NCS restraints were applied throughout refinement.

3. Results

3.1. Structure of Dsk2 UBL

The Dsk2 UBL domain structure was solved by molecular replacement at 1.15 Å resolution (Fig. 2*a*). The structure comprises a five-stranded β-sheet, one α-helix and one 3_{10}-helix (Fig. 2*b*). The total molecular surface area is 3811 Å^2. Dsk2 UBL is similar to other UBLs (reviewed in Walters *et al.*, 2004). Comparison with the NMR structures of HHR23A UBL (PDB code 1p98) and HHR23B UBL (PDB code 1p1a) show r.m.s.d.s of 1.7 and 1.6 Å, respectively. Secondary structures superimpose very well, whereas the loop regions differ (see supplementary material[1]). The structure is also similar to that of Ub (Ramage *et al.*, 1994; r.m.s.d. for 73 CA atoms 1.4 Å), but there are significant differences. In particular, the end of β1 and the loop to β2 have different conformations. The Ub residue L8, which is important for Ub recognition by UBA domains, is not conserved. Dsk2 residues S9 and G10 take different positions to Ub L8 and there is no corresponding hydrophobic interacting residue (Figs. 2*c* and 2*d*). The Dsk2 UBL domain, in common with other UBL domains and Ub, has a non-polar surface created by I45, I50, H69 and V71. The Dsk2 UBL is organized around a hydrophobic core that includes residues I5, I7, V16, V18, V24, F27, A30, I31, Y46, V57 and V68. These residues are similar in other UBL domains and in Ub (Fig. 2*d*).

A number of NMR studies have defined the interactions between human UBL domains and Ub and the two UIM motifs of the human proteasomal subunit S5a (Fujiwara *et al.*, 2003; Mueller & Feigon, 2003; Walters *et al.*, 2002, 2004; Wang *et al.*, 2005). These have shown similar interactions of the non-polar surface of the UBL or Ub molecules with residues with the sequence motif L*XX*AΦ*XX*S (where Φ is a bulky non-polar residue). The interactions are not strong, being represented by K_d values of >70 μM and often of several hundred μM. Rpn10, the *S. cerevisiae* subunit corresponding to human S5a, does not bind to Dsk2, although it does include the first UIM-binding site that has been shown to mediate the interaction between S5a and the human Dsk2 orthologue PLIC-2. Instead, the UBL domains of Rad23 and Dsk2 interact with the subunit Rpn1, a component of the base of the 19S proteasomal regulatory particle. This interaction is mediated by the Rpn1 leucine-rich region residues 417–627, which contains a putative LALAL UIM motif (Elsasser *et al.*, 2002). Interestingly, Rpn1 appears to have more than one UBL-binding site, which suggests that it may act as a scaffold to assemble multiple proteins (Elsasser *et al.*, 2004). The structure of the Dsk2 UBL domain suggests that it could bind a UIM motif in a similar fashion to other UBL domains, but that subtle differences in residues surrounding the non-polar patch could contribute to differing specificities.

3.2. Structure of Dsk2 UBA

The crystal structure of the Dsk2 UBA domain, solved from SeMet MAD measurements, shows a compact globular fold composed of a short one-turn helix α0 and three α-helices α1, α2 and α3 (Fig. 3*a*). The diameter is approximately 21 Å and the molecular surface area is 2608 Å^2. The inclination angles for the helix axes of α1 and α2, α1 and α3, and α2 and α3 are ~-60, ~-50 and $\sim-60^{\circ}$, respectively, and are close to the preferred α-helix packing for 'ridges into grooves'. Residues from all three helices (α1, Y332, I336, L339; α2, F347, N350,

V351, A353, L354; α3, V361, A364, L365 and L368) pack together to form a hydrophobic core. A Dsk2 UBA structure was recently solved by NMR as a component of a UBA–Ub complex (Ohno *et al.*, 2005). The UBA domains from X-ray and NMR structures superimpose with an r.m.s.d. of 0.7 Å for 47 C^{α} atoms (see supplementary material[1]).

The Dsk2 UBA molecule has a distinct charge polarity. The surface electrostatic potential reveals one negatively charged region composed of residues E329, E330 (α0), E333 (α1) and D348 (α2) and a second positively charged region created by residues R331 (α0), R355 and R356 (α2) (Figs. 3*a* and 3*b*). In the crystal structure, the two oppositely charged surfaces interact to form dimers and higher polymers arranged in a helical structure. These charged residues are not conserved in other UBA domains (Fig. 3*c*).

The contact residues at the interface between two UBA domains comprise residues from α0, α2, the loop α2/α3 and α3 and residues from α0, α1, the loop α1/α2 and α2 of the adjacent chain (Fig. 3*a*). In addition to the charge-mediated interactions, they include some non-polar interactions. For example, F345 packs against the aliphatic part of Q362 and F347 packs against the aliphatic part of R356 of the neighboring molecule. On average, the assembly results in a change of molecular-surface area of 944 Å^2 (472 Å^2 on each molecule), corresponding to 18% of the UBA molecular-surface area.

The Dsk2 UBA crystal asymmetric unit contains nine UBA molecules arranged as two chains: a pentamer (molecules *ABCDI*) and a tetramer (molecules *EFGH*), with molecule *C* contacting molecule *H* at the point where the two chains come together. Adjacent UBA domains in the chains are arranged in a helical structure characterized by a translation of 19.7 Å and a rotation of 40°. The lattice operations of the *C*2 symmetry generate remarkable continuous ninefold helices that extend throughout the crystal lattice (Fig. 4*a*). The interactions of the UBA molecules in the ninefold helices leave the putative Ub-binding residues solvent-exposed. However, at the interface between the two chains the interactions between molecules *H* and *C* block part of the Ub-binding site.

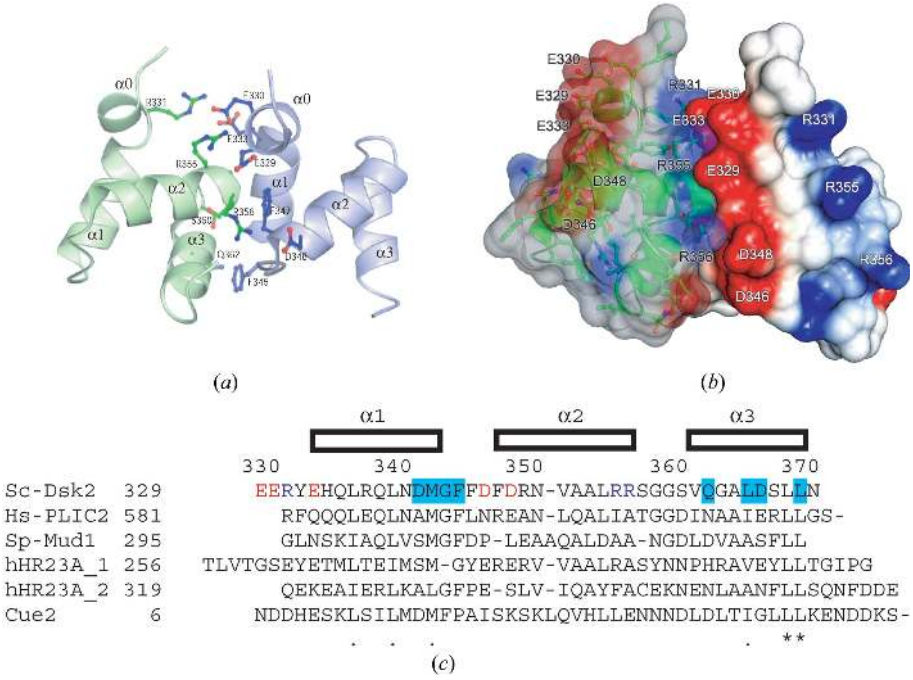

Figure 3
The structure of the Dsk2 UBA domain. (*a*) Details of the interactions at the Dsk2 UBA–UBA interface. Secondary-structural elements are labelled: α0, V327–R332; α1, E333–M342; α2, F347–R356; α3, G361–L369. See text for further details. (*b*) The association of two UBA molecules involves electrostatic interactions. van der Waals surface representation of two UBA molecules with electrostatic potential superimposed (figure produced with electrosurface routine in *AESOP*; J. Gruber & M. E. M. Noble, unpublished program). The view is similar to that of Fig. 3(*a*). The left molecule has a transparent surface to show the UBA secondary structure and side chains are in green. The Dsk2 UBA molecule has an asymmetric charge distribution with a cluster of negatively charged residues to the left (E329, E330, E333, D346 and D348) and a cluster of positively charged residues to the right (R331, R355 and R356). The complementary charged surfaces interact in the crystal to form helical polymers. (*c*) Structure-based sequence comparison for UBA domains from *S. cerevisiae* Dsk2, human PLIC2, *Schizosaccharomyces pombe* Mud1, human HR23A UBA domains 1 and 2 and *S. cerevisiae* Cue2. Secondary-structure elements for Dsk2 UBA are indicated. The negatively and positively charged residues that form the interacting surfaces for Dsk2 UBA polymers are indicated in red and blue, respectively. These residues are not conserved in other UBA domains. Residues that contact UBL in the UBA–UBL complex are highlighted in cyan.

3.3. Dsk2 UBA–UBL structure

The Dsk2 UBA–UBL complex structure was solved by molecular replacement using a tetramer of UBA molecules from the Dsk2 UBA structure as the search object. There are 18 copies of the UBA molecule per asymmetric unit. The UBA molecules are arranged in long helical chains, generated by the crystal lattice operations of $P2_1$ symmetry on the chains *ABCDEFGHI*, *JKLM* and *NOPQR* of the asymmetric unit. The lattice operations generate two chains *ABCDEFGHIA′B′ etc*. (where superscript prime indicates a lattice-related molecule) and *JKLMN′O′P′Q′R′ etc*. The chains have the same helical parameters (namely, rotation 40°, translation 19.7 Å) as observed in the native UBA structure and again a ninefold helix is generated (Fig. 4*b*). Although the UBA and UBL domains were crystallized in a 1:1 molar ratio, there are only three copies of the UBL domain in the asymmetric unit. The observation is explained by the unusual packing of the UBA molecules in the crystal lattice, which means that not every UBA molecule is available for interaction with a UBL molecule. Two of the UBL molecules are well ordered, but the third is less well ordered. The UBL molecules make contacts to the UBA molecules to form a 1:1 UBA–

UBL complex (Fig. 4*b*). The two well ordered UBL molecules each make a few contacts to two further UBA molecules from adjacent chains (Fig. 4*c*), while the third contacts only one other UBA molecule. It appears that the UBA–UBL association is weak and that the packing of adjacent chains reinforces binding in the crystal. These lattice contacts would not be available to reinforce binding in solution and indeed surface plasmon resonance data (discussed below) show that UBA–UBL binding is weak. The conformations of the individual UBA and UBL domains were restrained to those observed in the uncomplexed crystal structures. There were no indications of conformational changes for either the UBA or UBL domains.

UBA residues from the C-terminal end of α1, the α1/α2 loop and α3 helix contribute to the UBA–UBL interface. These residues contact the β-sheet of UBL in the region of β-strands 3, 4 and 5 (Figs. 2*d*, 3*c* and 5*a*). The crucial residues from the UBA include the MGF triplet, M342, G343 and F344, from the end of α1 that has previously been implicated in UBA/Ub binding. M342 (UBA) makes van der Waals contacts with I45, H69 and V71 from the UBL domain, the non-polar pocket identified from the UBL structure as part of a possible interaction region, while G343 and F344 (UBA) contact G48 (UBL) (Fig. 5*b*). The aromatic ring of UBA F344 stacks coplanar with the peptide bond between residues 48 and 49 of the UBL. These hydrophobic interactions are reinforced by contacts between L365 (UBA) and V71 (UBL) and between L369 (UBA) and I50 (UBL). There is one hydrogen bond between the main-chain O atom of UBA M342 and the main-chain N atom of UBL G48 and an ionic interaction between UBA D366 and UBL R43. The end of the UBA α1 helix is stabilized by a 3_{10}-turn hydrogen bond between the main-chain O atom of N340 and the main-chain N atom of G343; additionally, the main-chain O atom of F344 hydrogen bonds to the side chain of N350.

The side chain of M342 fits snugly into a hydrophobic cavity on the UBL surface created by H69, I45 and V71 (Fig. 5*c*). The hydrophobic pocket is extended by I50 and contact residues also include UBA F344, L365 and L369 (Fig. 5*d*). The interface buries a total molecular surface of 611 Å^2, comprising 315 Å^2 UBA molecular-surface area (about 12% of the UBA surface area) and 296 Å^2 UBL molecular-surface area (about 8% of

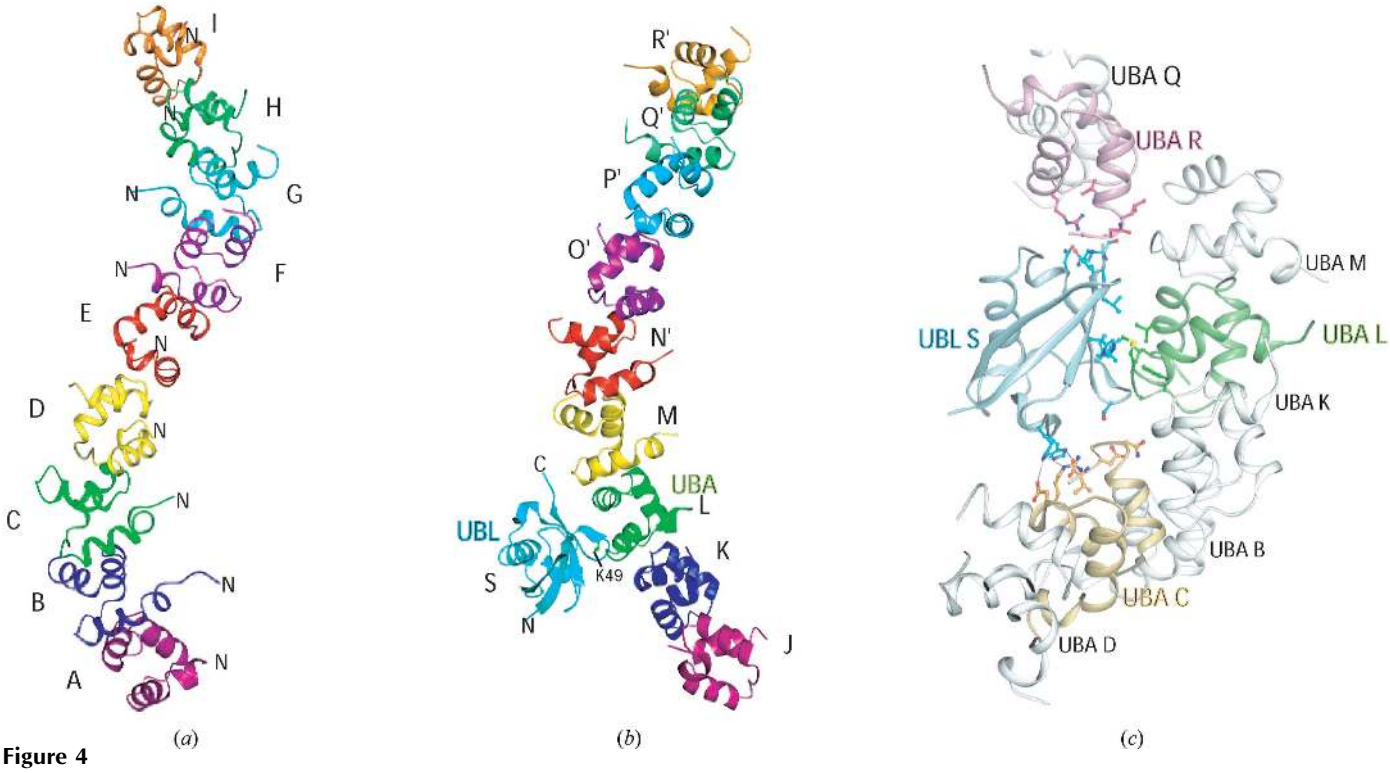

Figure 4
UBA domains associate into a ninefold helix in both the UBA and UBA–UBL crystals. (*a*) UBA domains associate to form a ninefold helix with successive rotations of 40° and translations of 19.7 Å. The UBA domains (molecules *ABCDEFGHI*) are colored magenta, blue, green, yellow, red and then purple, cyan, pale green, orange so that similar colours repeating every five molecules indicate a rotation of 200°. The N-termini of the domains are labelled. Their path indicates the helical twist about the vertical axis. (*b*) View approximately 90° to that shown in (*a*) illustrating a UBL molecule (*S*) associated with the UBA domain (*L*) in the UBA–UBL complex for the chain *JKLMN′O′P′Q′R′*, where a prime indicates a symmetry-related molecule. The chain has been tilted about the horizontal axis in order to show the position of UBL K49. (*c*) The main contacts between UBL (molecule *S*) and UBA (molecule *L*) in the chain *JKLMN′O′P′Q′R′* (where a prime indicates a symmetry-related molecule) are enhanced by minor contacts from UBL (*S*) to UBA (*C*) from the chain *ABCDEFGHI* and by minor contacts from UBL (*S*) to UBA (*R*) from the chain *NOPQR*. The *S* to *R* interface involves UBL residues N41, K72, S73, Q74 and UBA residues R349, L368, L369, N370 and G371. The *S* to *C* interface involves UBL residues S47, H61 and Q63 and UBA residues D346, R349, N370, G371, D372 and V373 with three hydrogen bonds: from UBL H61 side chain to UBA V373 C-terminal carboxylate, from UBL Q63 side-chain amide group to UBA D346 side-chain carboxylate and from UBL Q63 side-chain carbonyl group to UBA R349 NE group. The total molecular-surface area buried at the *S*–*R* contact is 304 Å^2, at the *S*–*C* interface is 327 Å^2 and at the *S*–*L* interface is 611 Å^2. Similar contacts are observed for the interactions of the UBL *T* molecule with UBA *D*, UBA *K* and UBA *A′*.

the UBL surface area). These areas are smaller than those buried at the UBA–UBA interface (described above) and are consistent with the low binding affinity between UBA and UBL (see below). In summary, the UBA–UBL interface is largely non-polar in nature, with one hydrogen bond and one ionic contact providing specificity for the binding.

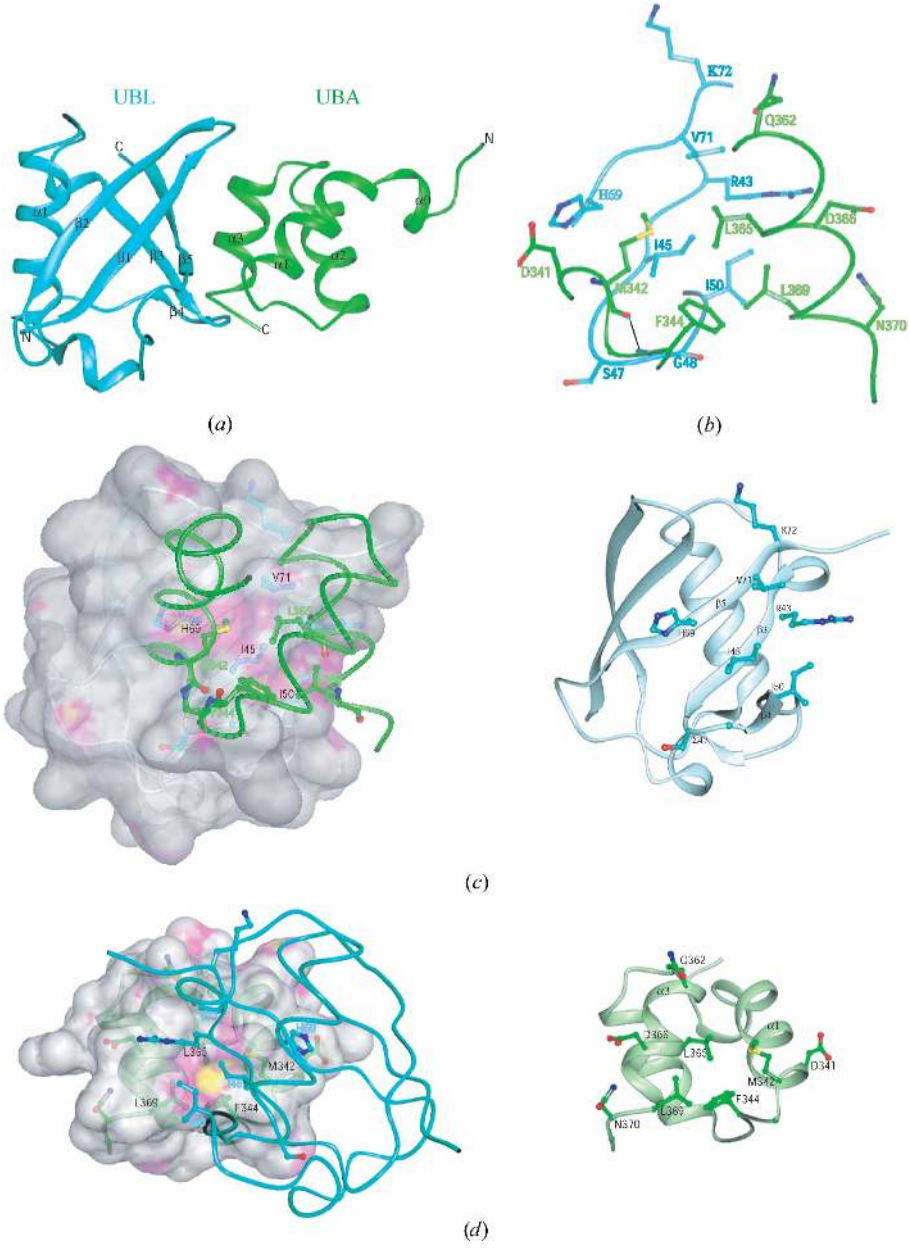

Figure 5
Contacts at the UBA–UBL interface. (*a*) Schematic representation of UBL (cyan) and UBA (green) showing the contact regions between UBA residues from the end of α1 helix, the α1/α2 loop and the α3 helix with residues from UBL from the β3, β4 and β5 strands. (*b*) Details of the contacts using the same colouring scheme as in (*a*). All residues from UBA and UBL that make contacts of <4.5 Å are shown. These are UBA residues D341, M342, G343, F344, Q362, L365, D366, L369 and G371 and UBL residues R43, I45, S47, G48, I50, H69, V71 and K72. The view is rotated ~90° about the vertical axis from (*a*). (*c*) The van der Waals surface of UBL as seen by the UBA molecule with the UBA molecule and interacting residues superimposed. The hydrophobic potential (Goodford, 1985) of the surface is coloured with the deepest hydrophobicity yellow, the middle range in magenta and the surface with neutral hydrophobic potential in grey (J. Gruber & M. E. M. Noble, unpublished work). The surface has been made partially transparent to reveal the UBL structure and interacting residues. The UBL structure without the surface is shown on the right. The view is similar to (*b*) and 90° from (*a*). (*d*) A view 180° from (*c*) showing the van der Waals surface of UBA as seen by the UBL molecule, with the UBL molecule and interacting residues superimposed. The colouring is as in (*c*). The UBA molecule without the surface is shown on the right.

3.4. Binding studies with surface plasmon resonance

The relative affinities of the purified Dsk2 UBA domain for Ub and Dsk2 UBL domain were measured with surface plasmon resonance. The Dsk2 UBA domain binds Dsk2 UBL with an affinity (K_d = 80 ± 15 μM) that is tenfold lower than that for Ub (K_d = 8 ± 3.5 μM) (see supplementary material[1]). The apparent affinities are likely to be higher than those observed for protein–protein interactions in solution because one component is immobilized. The affinities may also be overestimated because of the dimeric nature of the GST fusion and because of the relatively high levels of ligand captured, both of which can lead to rebinding of analyte during the dissociation phase (Raasi *et al.*, 2004). Nevertheless, the relative K_d values indicate clearly a higher affinity of the UBA domain for Ub than for UBL.

3.5. Why does Ub bind with greater affinity than UBL to the Dsk2 UBA domain?

The surface plasmon resonance data indicate that the UBL domain binds less well than Ub to the UBA domain. We compared the structures of our Dsk2 UBA–UBL complex with that of the Dsk2 UBA–Ub complex determined by NMR (Ohno *et al.*, 2005; Fig. 6*a*). Overall, the two UBA domains correspond closely (r.m.s.d. 0.7 Å) and the UBL and Ub molecules superimpose with an r.m.s.d. of 1.4 Å for 71 CA atoms. However, there are slight differences in the relative orientation of the molecules in the complex that result in an overall r.m.s.d. of 1.7 Å between the UBA–UBL and the UBA–Ub complexes. Nevertheless, the interactions at the interface, especially those made by the UBA MGF motif, are very similar (see supplementary material[1] and Fig. 6*b*). The most notable differences between the Dsk2 UBL domain and Ub

are the differences in conformation and sequence around Dsk2 S9, which is equivalent to Ub L8 (Fig. 2*c*). At the $\beta1/\beta2$ loop the Dsk2 UBL structure adopts a different conformation to that observed for Ub and there are no contacts to the UBA domain that mimic those made by Ub L8 to Dsk2 UBA (Fig. 6). The Ub residues 6–10 also contact the UBA with four potential hydrogen bonds (see supplementary material[1]). There are no corresponding contacts to these made in the UBA–UBL complex. However, to compensate, some interactions appear to be more intimate in the UBA–UBL complex. For example, L365 contacts I45 and V71 in the UBA–UBL complex but the contact distances are longer in the UBA–Ub complex. In addition, I50 in the UBL contacts UBA L369 but the corresponding Ub residue, Q49, makes no van der Waals interactions to the UBA. In other systems L8 is crucial to binding (Raasi *et al.*, 2004). Overall, the molecular surface buried in the UBA–Ub complex is greater (764 Å^2) compared with that buried in the UBA–UBL complex (611 Å^2), largely because of contacts in the region of Ub residues 6–10. We conclude that loss of the L8 contact and those of the residues surrounding L8 probably account for the lower affinity of Dsk2 UBA for UBL than for Ub.

3.6. Modelling of Ub onto adjacent UBA domains

A striking feature of the UBA chains seen in the crystal structures is the solvent accessibility of the Ub/UBL-binding site. To determine whether Ub could bind to adjacent UBA domains without steric hindrance, four Ub molecules (Vijay-Kumar *et al.*, 1987) were modelled onto a UBA tetramer by superimposing one of the Ub molecules onto the position of the UBL observed in the UBA–UBL complex structure and generating successive Ub molecules by applying the ninefold helical transformation. The C-terminal region of Ub, which is flexible (Ohno *et al.*, 2005), was adjusted to a position similar to the position it adopts in the Ub_2 crystal structure (Cook *et al.*, 1992). The model showed that such an assembly is stereochemically reasonable. The UBA/Ub-binding interfaces are maintained without any clashes and some favourable contacts between adjacent Ub molecules (Figs. 7*a* and 7*b*). In the model, the Ub K48 side chain is close to the C-terminus of an adjacent Ub molecule and a flexible isopeptide link can be made. The side chains of other lysines (K6, K29 and K63) are distant from the C-termini and are unable to form the isopeptide bond. This model suggests a mechanism by which the Dsk2 UBA domains could selectively recognize K48-linked Ub molecules with high affinity (see §4).

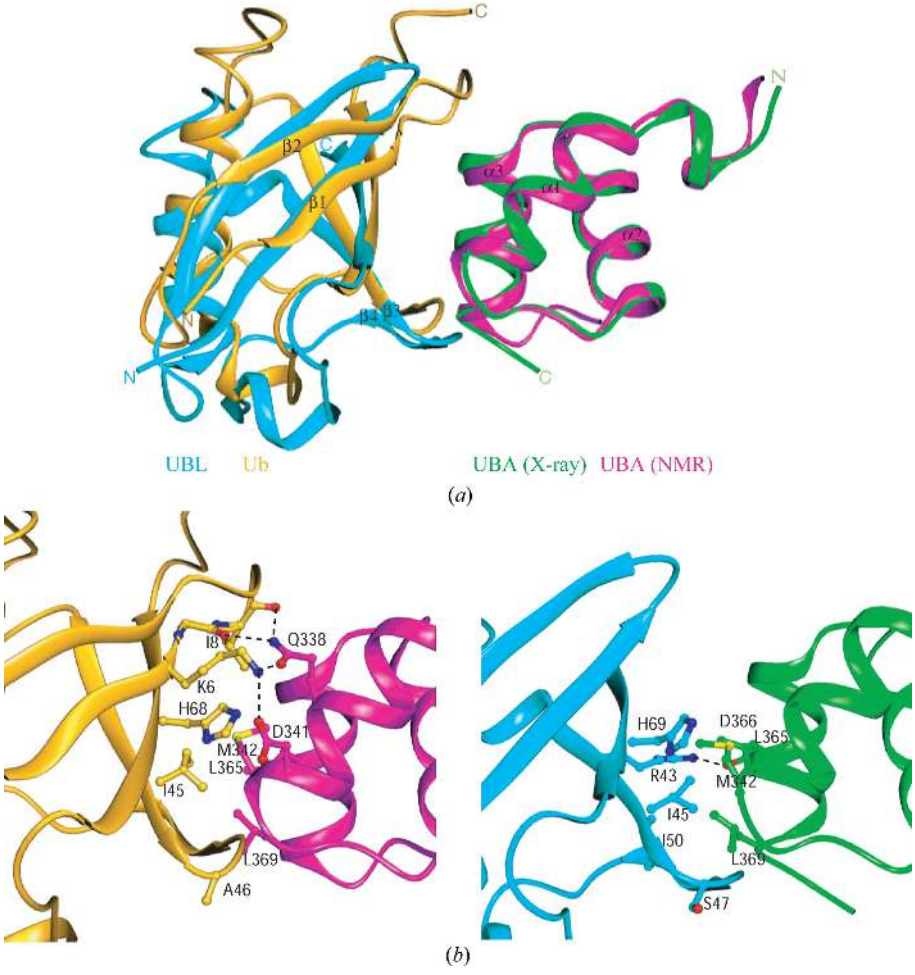

Figure 6
(*a*) Comparison of the Dsk2 UBA–UBL complex (green and cyan, respectively) with the Dsk2 UBA–Ub complex (magenta and orange, respectively; from Ohno *et al.*, 2005). The major differences at the interface are at the $\beta1/\beta2$ loop and the $\beta3/\beta4$ loop of UBL and Ub. Further details are described in the text. (*b*) A simplified view of the contacts between Ub (gold) and UBA (magenta) (left) and UBL (cyan) and UBA (green) (right) showing the domains in the same orientation as Fig. 6(*a*). Only the most significant contacts that differ between the two structures are shown. The Ub–UBA interface has contacts from Ub residues K6 and L8 to UBA residues which are not made in the UBBL–UBA complex. The UBL–UBA complex has closer contacts between I45 and I50 with UBA residues L365 and L369 that in the Ub–UBA complex. Full details of the contacts are given in the supplementary material.

4. Discussion

We have determined the crystal structures of the UBL and UBA domains of the *S. cerevisiae* Dsk2 protein both in their unbound state and in complex. The isolated domains share the canonical folds of their respective protein-fold families. In the crystals of the UBA domain and the UBA–UBL complex, the UBA domains assemble into ninefold helical chains utilizing a largely electrostatic binding interface. UBA domains associated in this way retain

the ability to bind UBL domains and by inference Ub.

The UBA–UBL structure is the first crystal structure of its type. Measurements with surface plasmon resonance indicate a tenfold higher affinity for UBA binding to Ub compared with UBL. By comparing the structures reported in this paper with the structure of Dsk2 UBA–Ub determined by NMR, we note that key interactions, which are mediated primarily by the MGF motif (342–344 in Dsk2 UBA), are conserved but that there are differences that result from sequence differences between Dsk2 UBL and Ub in the vicinity of L8. Loss of the L8 contribution in the UBA–UBL complex probably accounts for the higher affinity of the Dsk2 UBA domain for Ub than its UBL. We note that contacts observed in the Dsk2 UBA–UBL crystal structure are consistent with those inferred from an analysis of NMR chemical shift perturbation data of UBA interactions with Ub and UBL domains of the DNA damage-repair protein hHR23B (Ryu *et al.*, 2003).

The observation that the Dsk2 UBA and UBL domains can form a complex provides support for the notion that full-length Dsk2 may adopt a closed conformation mediated by intramolecular binding of its UBL and UBA domains. A similar proposal has been made for hHR23A (Walters *et al.*, 2003). The UBA–UBL interaction should be relatively weak and disruption must be possible to allow Ub and its chains to bind to the UBA domain. The structure of the complex (Fig. 4*b*) shows that the C-terminus of UBL and the N-terminus of UBA are free to make the connection through the intervening sequence in full-length Dsk2. Only when the UBA–UBL interaction is disrupted would the UBL domain be available for interaction with the proteasome, thus providing a mechanism whereby only Dsk2 molecules carrying 'cargo' would be targeted to the proteasome. This offers a regulatory mechanism for Dsk2 adapter function during delivery of polyubiquitinated substrates to the proteasome.

Varadan *et al.* (2005) reported a model for the recognition of Ub_2 by the UBA2 domain of hHR23A based on NMR titration and NOE measurements with mutagenesis data in which a 'closed' conformation of K48-linked Ub_2 formed a 1:1 complex with the UBA in a sandwich-like complex (Fig. 7*c*). A similar sandwich model has been proposed for the binding of UBA domain of the fission yeast Mud1 protein to K48-linked Ub_2 (Trempe *et al.*, 2005). The models implicate similar recognition surfaces for Ub_2 to those that had been observed in monoubiquitin hHR23A complexes but the UBA interacting surfaces are different. As described by Varadan *et al.* (2005), the UBA contact to the proximal Ub *via* α2 and the relative orientation of the UBA with respect to the distal Ub are different to those observed in previous monoubiquitin–UBA complexes. We asked whether the Dsk2 UBA domain was likely to bind to Ub_2 in a similar fashion by superimposing the UBA from the UBA–UBL crystal structure onto the HR23A UBA domain in the UBA–Ub_2 model. The UBA domains align with an r.m.s.d. of 1.6 Å for 39 atoms, showing the greatest differences in their N- and C-terminal regions and in the relative orientation of the α3 helices. The Dsk2 UBA could make contacts with the distal Ub of the HR23A model, although not as effectively in the Dsk2 UBA–Ub complex. However, there are significant changes in sequence in Dsk2 UBA compared with hHR23A and Mud1 that affect the

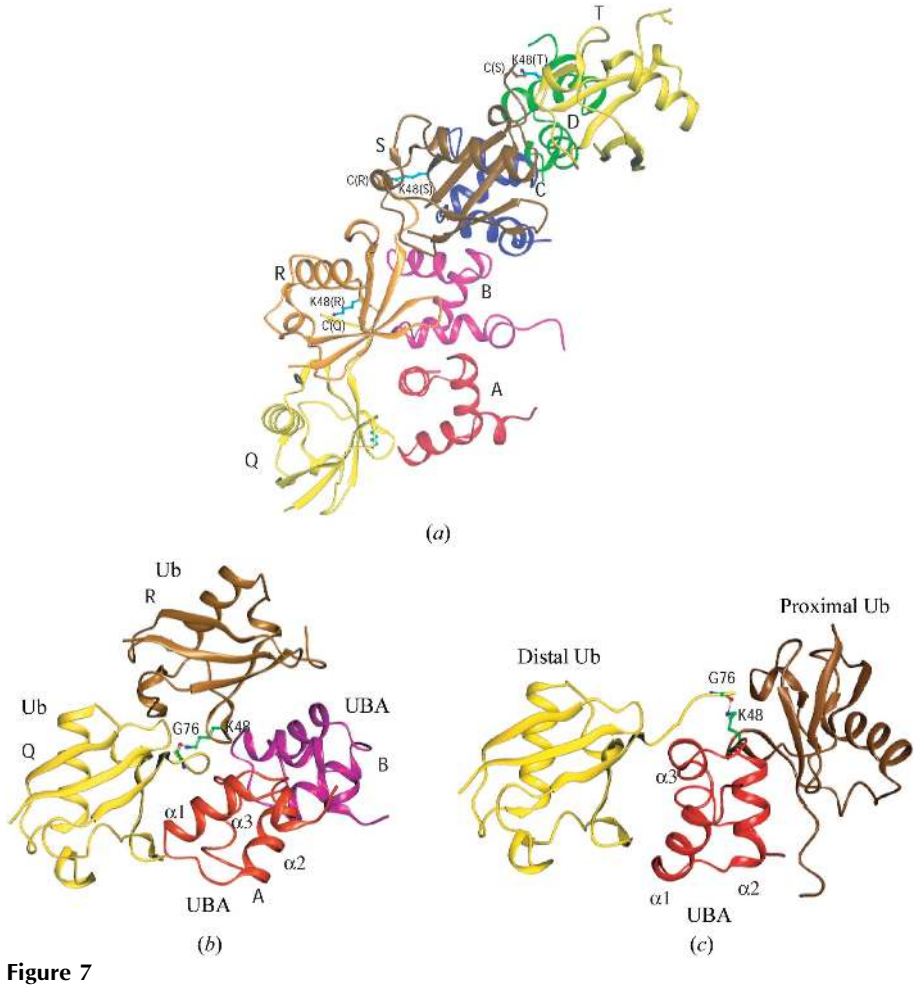

Figure 7
A model for tetraubiquitin (Ub_4) binding to four Dsk2 UBA molecules. (*a*) The Dsk2 UBA molecules, arranged in a ninefold helix as in the UBA/UBL crystal structure, are labelled *A*, *B*, *C* and *D* and coloured red, magenta, blue and green, respectively. The Ub_4 subunits, modelled on the UBL structure in the UBA–UBL complex, are labelled *Q*, *R*, *S*, *T* and colored yellow, orange, brown and yellow, respectively. They are linked by an isopeptide bond from the C-terminal G76 of one Ub molecule to K48 (shown in cyan) of the neighboring Ub molecule. (*b*) An enlarged view of the Dsk2 UBA dimer associated with the modelled Ub_2 showing the C-terminal G76–K48 linker. (*c*) The HR23A UBA–Ub_2 complex from Varadan *et al.* (2005) with the distal Ub molecule oriented as in the Ub molecule *Q* in (*b*). The diagram illustrates the different modes of association of the different UBA domains and the flexibility of the G76–K48 linker.

proximal Ub-binding site. Notably, the changes from Q339, F342 and A343 in the HR23A UBA to A352, R355 and R356 in Dsk2 UBA domain not only remove favorable interactions but also provide steric clashes that would prevent binding. It may be that Dsk2 differs from both HR23A and Mud1 in its mechanism of Ub-chain binding. Our structures of the UBA and UBA–UBL complex has led to an alternative model (Figs. 7*a* and 7*b*). In this model, it is proposed that K48-linked Ub molecules could act as a scaffold to recruit the assembly of non-covalently linked Dsk2 UBA domains. The individual UB–Ub binding affinities would be supplemented by the UBA–UBA interactions to give a cooperative binding mechanism. Only Ub chains linked *via* K48 have the appropriate topology to enable simultaneous binding to successive UBA domains. K48-linked Ub chains are the most abundant form of poly-UB in cells and the model is consistent with the results of Funakoshi *et al.* (2002). Recent work has shown that Dsk2 UBA domains have no preference for chain linkage, but in these experiments the immobilization of GST-UBA would not allow the assembly of the complex proposed here.

Since this manuscript was submitted, Sasaki *et al.* (2005) report from yeast two-hybrid studies that Dsk2 can form homodimers *via* its C-terminal UBA domain. A truncated C-terminal UBA domain (residues 336–373) was not able to bind to full-length Dsk2. The residues deleted in this truncated UBA domain include just those that in the crystal structure are important for UBA associations into the helical ribbons seen in the crystal lattice (namely E329, E330, R331 and E333: Fig. 3). Moreover, in an analysis of *in vivo* yeast extracts, Sasaki and coworkers report that higher molecular-weight Dsk2 fractions are observed in sucrose-density centrifugations and that these fractions bind polyubiqutin, while little binding of polyubiquitin was observed for monomeric Dsk2 and neither monomeric Dsk2 nor the higher molecular-weight fractions bound monomeric Ub. Finally, in growth-rescue experiments it was shown that the Dsk2 UBA domain is essential for Dsk2 function. These recent results are consistent with the model described in this manuscript, in which it is proposed that the ability of Dsk2 UBA domains to associate could be important for the biological function of Dsk2 in the delivery of polyubiqitinated targets to the proteasome. The model also implies that the association of UBA domains to Ub chains in the full-length Dsk2 molecule will result in more than one UBL domain being available for interaction with the 19S regulatory particle, providing an opportunity for cooperative binding of target-loaded Dsk2 to the proteasome. However, we note that most UBA domains do not have charged residues corresponding to those that mediate the electrostatic interactions of the Dsk2 UBA helical structures. It may be that Dsk2 is unique. For these reasons, we remain cautious about the universality of the proposed model. Structural and functional studies have been initiated to assess the validity of the model.

We warmly thank Neil Oldham and Robin Aplin for help with mass spectrometry, Jan Gruber, Kazuhiro Iwai, Hideki Kobayashi for the gift of vectors, Tony Willis for N-terminal sequencing and Simon Holton for data processing. We thank the beamline staff at ESRF, Grenoble, who provided excellent facilities for the X-ray measurements. This work has been funded by grants from the MRC, the Wellcome Trust and the Arab Fund Fellowships Program.

References

Bertolaet, B. L., Clarke, D. J., Wolff, M., Watson, M. H., Henze, M., Divita, G. & Reed, S. I. (2001). *Nature Struct. Biol.* **8**, 417–422.
Biggins, S., Ivanovska, I. & Rose, M. D. (1996). *J. Cell Biol.* **133**, 1331–1346.
Chau, V., Tobias, J. W., Bachmair, A., Marriott, D., Ecker, D. J., Gonda, D. K. & Varshavsky, A. (1989). *Science*, **243**, 1576–1583.
Ciani, B., Layfield, R., Cavey, J. R., Sheppard, P. W. & Searle, M. S. (2003). *J. Biol. Chem.* **278**, 37409–37412.
Collaborative Computational Project, Number 4 (1994). *Acta Cryst.* D**50**, 760–763.
Cook, W. J., Jeffrey, L. C., Carson, M., Chen, Z. & Pickart, C. M. (1992). *J. Biol. Chem.* **267**, 16467–16471.
Davies, G. C., Ettenberg, S. A., Coats, A. O., Mussante, M., Ravichandran, S., Collins, J., Nau, M. M. & Lipkowitz, S. (2004). *Oncogene*, **23**, 7104–7115.
Dieckmann, T., Withers-Ward, E. S., Jarosinski, M. A., Liu, C. F., Chen, I. S. & Feigon, J. (1998). *Nature Struct. Biol.* **5**, 1042–1047.
Elsasser, S., Chandler-Militello, D., Muller, B., Hanna, J. & Finley, D. (2004). *J. Biol. Chem.* **279**, 26817–26822.
Elsasser, S., Gali, R. R., Schwickart, M., Larsen, C. N., Leggett, D. S., Muller, B., Feng, M. T., Tubing, F., Dittmar, G. A. & Finley, D. (2002). *Nature Cell Biol.* **4**, 725–730.
Ferrell, K., Wilkinson, C. R., Dubiel, W. & Gordon, C. (2000). *Trends Biochem. Sci.* **25**, 83–88.
Foadi, J., Woolfson, M. M., Dodson, E. J., Wilson, K. S., Jia-xing, Y. & Chao-De, Z. (2000). *Acta Cryst.* D**56**, 1137–1147..
Fujiwara, K., Tenno, T., Sugasawa, K., Jee, J., Ohki, I., Kojima, C., Tochio, H., Hiroaki, H., Hanaoka, F. & Shirakawa, M. (2003). *J. Biol. Chem.* **279**, 4760–4767.
Funakoshi, M., Geley, S., Hunt, T., Nishimoto, T. & Kobayashi, H. (1999). *EMBO J.* **18**, 5009–5018.
Funakoshi, M., Sasaki, T., Nishimoto, T. & Kobayashi, H. (2002). *Proc. Natl Acad. Sci. USA*, **99**, 745–750.
Goodford, P. J. (1985). *J. Med. Chem.* **28**, 849–858.
Groll, M., Ditzel, L., Lowe, J., Stock, D., Bochtler, M., Bartunik, H. D. & Huber, R. (1997). *Nature (London)*, **386**, 463–471.
Hartmann-Petersen, R., Seeger, M. & Gordon, C. (2003). *Trends Biochem. Sci.* **28**, 26–31.
Hershko, A. & Ciechanover, A. (1998). *Annu. Rev. Biochem.* **67**, 425–479.
Hiyama, H., Yokoi, M., Masutani, C., Sugasawa, K., Maekawa, T., Tanaka, K., Hoeijmakers, J. H. & Hanaoka, F. (1999). *J. Biol. Chem.* **274**, 28019–28025.
Hofmann, K. & Bucher, P. (1996). *Trends Biochem. Sci.* **21**, 172–173.
Jones, T. A., Zou, J. Y., Cowan, S. W. & Kjeldgaard, M. (1991). *Acta Cryst.* A**47**, 110–119.
Kang, R. S., Daniels, C. M., Francis, S. A., Shih, S. C., Salerno, W. J., Hicke, L. & Radhakrishnan, I. (2003). *Cell*, **113**, 621–630.
Kaye, F. J., Modi, S., Ivanovska, I., Koonin, E. V., Thress, K., Kubo, A., Kornbluth, S. & Rose, M. D. (2000). *FEBS Lett.* **467**, 348–355.
Kleijnen, M. F., Alarcon, R. M. & Howley, P. M. (2003). *Mol. Biol. Cell*, **14**, 3868–3875.
La Fortelle, E. de & Bricogne, G. (1997). *Methods Enzymol.* **276**, 472–494.
Leslie, A. G. W. (1999). *Acta Cryst.* D**55**, 1696–1702.
Madura, K. (2004). *Trends Biochem. Sci.* **29**, 637–640.

Masutani, C., Araki, M., Sugasawa, K., van der Spek, P. J., Yamada, A., Uchida, A., Maekawa, T., Bootsma, D., Hoeijmakers, J. H. & Hanaoka, F. (1997). *Mol. Cell. Biol.* **17**, 6915–6923.
Mueller, T. D. & Feigon, J. (2002). *J. Mol. Biol.* **319**, 1243–1255.
Mueller, T. D. & Feigon, J. (2003). *EMBO J.* **22**, 4634–4645.
Mueller, T. D., Kamionka, M. & Feigon, J. (2004). *J. Biol. Chem.* **279**, 11926–11936.
Murshudov, G. N., Vagin, A. A. & Dodson, E. J. (1997). *Acta Cryst.* D**57**, 240-255.
Navaza, J. (1994). *Acta Cryst.* A**50**, 157–163.
Nocker, S. van, Sadis, S., Rubin, D. M., Glickman, M., Fu, H., Coux, O., Wefes, I., Finley, D. & Viestra, R. D. (1996). *Mol. Cell. Biol.* **16**, 6020–6028.
Ohno, A., Jee, J., Fujiwara, K., Tenno, T., Goda, N., Tochio, H., Kobayashi, H., Horoaki, H. & Shirakawa, M. (2005). *Structure*, **13**, 521–532.
Peng, J., Schwartz, D., Elias, J. E., Thoreen, C. C., Cheng, D., Marsischky, G., Roelofs, J., Finley, D. & Gygi, S. P. (2003). *Nature Biotechnol.* **21**, 921–926.
Pickart, C. M. (2001). *Annu. Rev. Biochem.* **70**, 503–533.
Prag, G., Misra, S., Jones, E. A., Ghirlando, R., Davies, B. A., Horazdovsky, B. F. & Hurley, J. H. (2003). *Cell*, **113**, 609–620.
Raasi, S., Orlov, I., Fleming, K. G. & Pickart, C. M. (2004). *J. Mol. Biol.* **341**, 1367–1379.
Raasi, S., Varadan, R., Fushman, D. & Pickart, C. (2005). *Nature Struct. Mol. Biol.* **12**, 708–714.
Ramage, R., Green, J., Muir, T. W., Ogunjobi, O. M., Love, S. & Shaw, K. (1994). *Biochem. J.* **299**, 151–158.
Rao, H. & Sastry, A. (2002). *J. Biol. Chem.* **277**, 11691–11695.
Rao-Naik, C., delaCruz, W., Laplaza, J. M., Tan, S., Callis, J. and Fisher, A. J. (1998). *J. Biol. Chem.* **273**, 34976–34982.
Ryu, K. S., Lee, K. J., Bae, S. H., Kim, B. K., Kim, K. A. & Choi, B. S. (2003). *J. Biol. Chem.* **278**, 36621–36627.
Sasaki, T., Funakoshi, M., Endicott, J. A. & Kobayashi, H (2005). *Biochem. Biophys. Res. Commun.* **336**, 530–535.
Saeki, Y., Sone, T., Toh-e, A. & Yokosawa, H. (2002). *Biochem. Biophys. Res. Commun.* **296**, 813–819.
Schauber, C., Chen, L., Tongaonkar, P., Vega, I., Lambertson, D., Potts, W. & Madura, K. (1998). *Nature (London)*, **391**, 715–718.
Schneider, T. R. & Sheldrick, G. M. (2002). *Acta Cryst.* D**58**, 1772–1779.
Seeger, M., Hartmann-Petersen, R., Wilkinson, C. R., Wallace, M., Samejima, I., Taylor, M. S. & Gordon, C. (2003). *J. Biol. Chem.* **278**, 16791–16796.
Terwilliger, T. C. (2000). *Acta Cryst.* D**56**, 965–972.
Thrower, J. S., Hoffman, L., Rechsteiner, M. & Pickart, C. M. (2000). *EMBO J.* **19**, 94–102.
Trempe, J.-F., Brown, N. R., Lowe, E. D., Noble, M. E. M., Gordon, C., Campbell, I. D. & Endicott, J. A. (2005). *EMBO J.* **24**, 3178–3189.
Vagin, A. & Teplyakov, A. (1997). *J. Appl. Cryst.* **30**, 1022–1025.
Varadan, R., Assfalg, M., Raasi, S., Pickart, C. & Fushman, D. (2005). *Mol. Cell*, **18**, 687–698.
Vijay-Kumar, S., Bugg, C. E. & Cook, W. J. (1987). *J. Mol. Biol.* **194**, 531–544.
Walters, K. J., Goh, A. M., Wang, Q., Wagner, G. & Howley, P. M. (2004). *Biochim. Biophys. Acta*, **1695**, 73–87.
Walters, K. J., Kleijnen, M. F., Goh, A. M., Wagner, G. & Howley, P. M. (2002). *Biochemistry*, **41**, 1767–1777.
Walters, K. J., Lech, P. J., Goh, A. M., Wang, Q. & Howley, P. M. (2003). *Proc. Natl Acad. Sci. USA*, **100**, 12694–12699.
Wang, Q., Goh, A. M., Howley, P. M. & Walters, K. J. (2003). *Biochemistry*, **42**, 13529–13535.
Wang, Q., Young, P. & Walters, K. J. (2005). *J. Mol. Biol.* **384**, 727–739.
Wilkinson, C. R., Seeger, M., Hartmann-Petersen, R., Stone, M., Wallace, M., Semple, C. & Gordon, C. (2001). *Nature Cell Biol.* **3**, 939–943.
Withers-Ward, E. S., Mueller, T. D., Chen, I. S. & Feigon, J. (2000). *Biochemistry*, **39**, 14103–14112.